Hindawi
International Journal of Antennas and Propagation
Volume 2023, Article ID 7943177, 7 pages
https://doi.org/10.1155/2023/7943177

Research Article

Design of a Bandpass Filter with Mixed Electromagnetic Coupling Paths Using Vertical Split-Ring Resonators

Jaehyuk Lim,[1,2] Hogeun Yoo,[1] and Jaehoon Lee[1]

[1]*Department of Computer Science and Engineering, Korea University, Anam-Dong, Seongbuk-Gu, Seoul 02841, Republic of Korea*
[2]*Agency for Defense Development, Yuseong, P.O. Box 35, Daejeon 34186, Republic of Korea*

Correspondence should be addressed to Jaehoon Lee; ejhoon@korea.ac.kr

Received 31 October 2022; Revised 6 April 2023; Accepted 28 April 2023; Published 10 May 2023

Academic Editor: Giuseppe Castaldi

Copyright © 2023 Jaehyuk Lim et al. This is an open access article distributed under the Creative Commons Attribution License, which permits unrestricted use, distribution, and reproduction in any medium, provided the original work is properly cited.

We propose bandpass filters (BPFs) with mixed electromagnetic coupling paths (MEMCPs) that comprise two coupled vertical split-ring resonators (VSRRs) and present the equivalent circuit models of the coupled VSRRs. We demonstrate that the dominant coupling modes for the top and bottom layers of the VSRRs are magnetic (M) and electric (E), respectively, and that M-dominant coupling is required for high-selectivity BPFs. BPFs with narrow and wide bandwidths were designed based on the generalized coupling matrix. The proposed BPFs were fabricated and measured, and it is verified that the proposed BPFs have high selectivity due to the transmission zeros and a small circuit footprint due to the vertical structure of resonators. The fabricated narrow- and wide-band BPFs have the fractional bandwidths of 3.62% and 5.81%, respectively, with the overall size of $0.29\lambda_g \times 0.043\lambda_g$.

1. Introduction

Planar-type metamaterials, such as split-ring resonators (SRRs) and complementary SRRs, are widely used in planar microwave devices, including bandstop filters (BSFs) and bandpass filters (BPFs), as they are simple to fabricate. However, these resonators are too large for use in modern communication systems and many studies have focused on reducing their electrical footprint [1–4], resulting in the introduction of spiral resonators (SRs) [1], broad-side coupling [2, 3], and hexagonal SRR [4]. Fundamental limits apply to the electrical size of resonators designed on a single plane. Therefore, geometries such as the vertical SRRs (VSRRs) were proposed [5–7], but filters constructed in this form have low selectivity.

Filter selectivity can be improved by introducing transmission zeros (TZs). In [8–13], high-selectivity BPFs were realized that utilized electromagnetic coupling paths (EMCPs) between resonators. These can either be mixed electromagnetic coupling paths (MEMCPs) [8–10, 13] or separated electromagnetic coupling paths (SEMCPs) [11, 12]. In [13], the triple mode resonator was used to design compact triple band BPFs, and their selectivity was improved by transmission zeros through MEMCPs. In [14], MEMCPs were applied to a dual-band filtering power divider to enhance its selectivity.

Here, we propose highly selective BPFs with coupling paths between two coupled VSRRs and derive the equivalent circuit. We show that the dominant coupling paths between the top and bottom layers of the VSRRs are magnetic (M) and electric (E), respectively. In order to adjust the amount of E-coupling and M-coupling, the distances between two VSRRs on the top and bottom layers were adjusted. Additional TZs are generated because of the mixed electromagnetic coupling paths (MEMCPs) between the coupled VSRRs, enabling the design of a BPF with high selectivity.

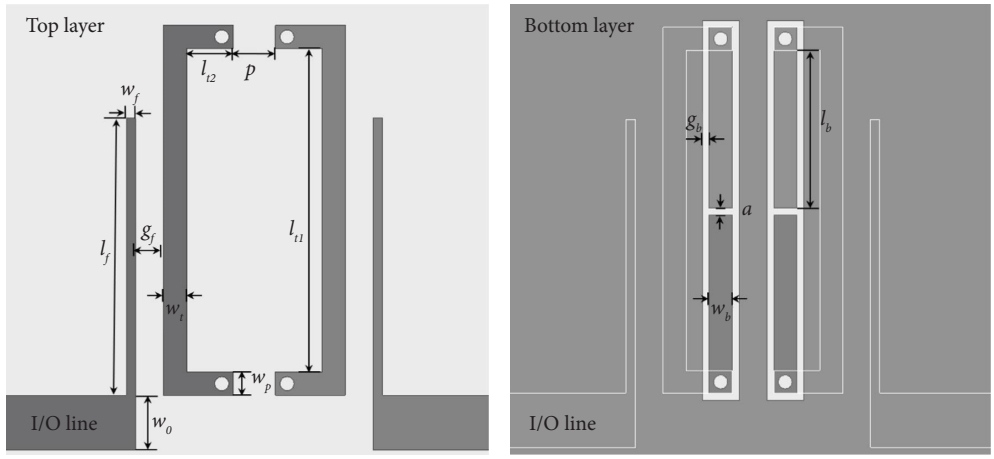

Figure 1: Top and bottom views of the proposed bandpass filter (BPF) comprising coupled vertical split-ring resonators (VSRRs).

2. Highly Selective Bandpass Filter Designs Using Two Coupled Vertical Split-Ring Resonators

2.1. Analysis of Coupling Paths between Two Coupled VSRRs. Figure 1 shows the proposed BPF, which comprises two coupled VSRRs and I/O lines; the top layer of the VSRR was defined using a microstrip line, and the bottom layer of the VSRR was defined using coplanar waveguides. Through-hole vias (radius = 0.25 mm) were used to connect the transmission lines on the top and bottom layers. As shown in Figure 2, the E- and H-field distributions of the proposed BPF were calculated at the resonant frequency ($f_r = 2.9$ GHz) for the given dimensions ($w_0 = 2.347$ mm, $w_t = w_b = w_p = 1$ mm, $l_{t1} = 18$ mm, $l_{t2} = 0$ mm, $g_b = a = 0.15$ mm, $p = 1.8$ mm, $w_f = 0.4$ mm, $g_f = 0.3$ mm, and $l_f = 15.2$ mm, $l_b = 8.9$ mm) including the properties of the Rogers 5880 substrate ($\varepsilon_r = 2.2$, height = 0.784 mm, loss tangent $\delta = 0.0009$) using ANSYS HFSS. The dimensional parameters of the single VSRR determine its resonant frequency [6]. As shown in Figure 2(a), the E-field was dominant in the bottom layer coplanar waveguides, and the H-field was dominant in the top layer microstrip line, as shown in Figure 2(b). As argued in [15], E-coupling and M-coupling are dominant for coplanar and microstrip waveguides, respectively; therefore, novel mixed electromagnetic coupling paths (MEMCPs) between two VSRRs are more easily realized compared to the previous methods [8–12], and MEMCP can be used to design BPFs with high selectivity. To control the levels of E-coupling and M-coupling, we adjusted the distances between the two VSRRs on the top and bottom layers. Specifically, the distance between the two VSRRs on the bottom layer was determined solely by the parameter p, whereas the distance between the two VSRRs on the top layer was modified by both p and l_{t2}.

Figure 3(a) shows the equivalent circuit model of the coupled VSRRs; L_r and C_r represent the inductance and capacitance of the VSRRs, respectively, and the resonant frequency of the VSRRs is $f_r = 1/2\pi\sqrt{L_r C_r}$. L_m and C_m are the mutual inductance and capacitance generated by M-coupling and E-coupling between the VSRRs, respectively. In Figure 3(b), the circuit is expressed in terms of the M-coupling impedances Z_{11} and Z_{12}, and the E-coupling admittances Y_{11} and Y_{12}, with respect to the reference plane. According to [15], Z_{11} and Z_{12} can be expressed as

$$Z_{11} = j\omega L_r, Z_{12} = j\omega L_m. \tag{1}$$

Similarly, Y_{11} and Y_{12} can be expressed as

$$Y_{11} = j\omega C_r, Y_{12} = -j\omega C_m. \tag{2}$$

As shown in Figure 3(c), it follows that the even- and odd-mode resonance frequencies f_e and f_o can be obtained by the following equation:

$$f_e = \frac{1}{\sqrt{(L_r + L_m)(C_r - C_m)}}, \quad f_o = \frac{1}{\sqrt{(L_r - L_m)(C_r + C_m)}}. \tag{3}$$

By incorporating (1) and (2), the coupling coefficient k can be expressed as

$$k = \frac{{f_o}^2 - {f_e}^2}{{f_o}^2 + {f_e}^2} \approx \frac{L_m}{L_r} - \frac{C_m}{C_r}, \tag{4}$$

when $L_m C_m \ll L_r C_r$. Finally, it follows that $k > 0$ when M-coupling is dominant ($f_o > f_e$) and $k < 0$ when E-coupling is dominant ($f_o < f_e$).

The dominant coupling mode of the proposed BPF (Figure 1) can be controlled by selection of l_{t2}. ANSYS HFSS was used to simulate the S-parameter S_{21} as a function of length l_{t2}, with weak coupling conditions ($w_f = 0.4$ mm, $g_f = 0.8$ mm, $l_f = 9$ mm); the results are plotted in Figure 4. The parameter l_{t2} represents the distance between the two VSRRs on the top layer, where the H-field is dominant. As a result, l_{t2} has a greater impact on M-coupling than on E-coupling and can be used to control the odd-mode resonant frequency while keeping the even-mode resonant frequency, as shown in Figures 4(a) and 4(b). As l_{t2} was increased, the value of L_m decreased, the values of L_r and C_r increased, therefore, f_o decreased. The f_e was 3.2 GHz and was

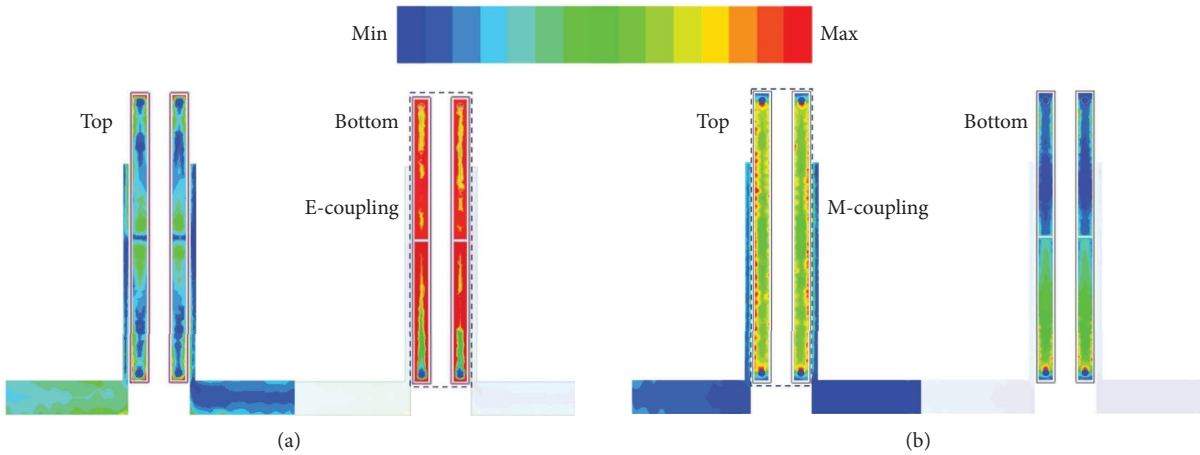

FIGURE 2: Field distributions E- and H-fields around the proposed BPF at the resonant frequency of 2.9 GHz ($l_{t2} = 0$ mm). (a) E-field distribution. (b) H-field distribution.

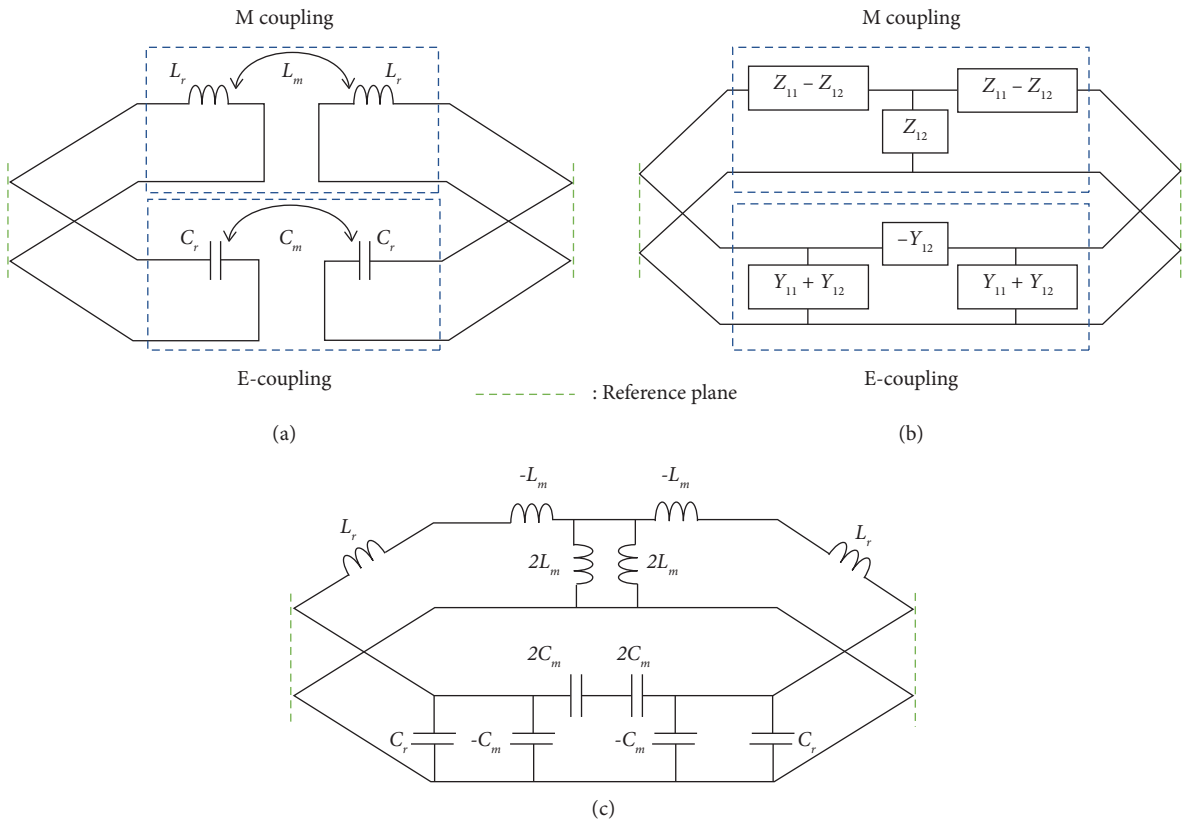

FIGURE 3: (a) Equivalent circuit model of coupled VSRRs, (b) equivalent circuit model with the M-coupling impedances and the E-coupling admittances, and (c) alternative circuit model of coupled VSRRs.

independent of the changes in l_{t2}; therefore, it can be deduced that the decrease of $(L_r + L_m)$ was similar to the increase of $(C_r - C_m)$.

As shown in Figure 4(a), two TZs are generated when M-coupling is dominant ($f_o > f_e$); one TZ is located at a frequency smaller than f_e, and the second TZ is greater than f_o by canceling the effects of E- and M-coupling [11]. There are no TZs when E-coupling is dominant ($f_o < f_e$), as illustrated in Figure 4(b). Therefore, it is critical to maintain M-dominant coupling between the VSRRs when designing a highly selective BPF.

2.2. Filter Design. Coupled VSRRs were used to design narrow- and wide-band second-order Chebyshev BPFs with a passband return loss (RL) less than 20 dB and a center-frequency of $f_c = 2.9$ GHz. The $N + 2$ general coupling matrix for a Chebyshev circuit model is

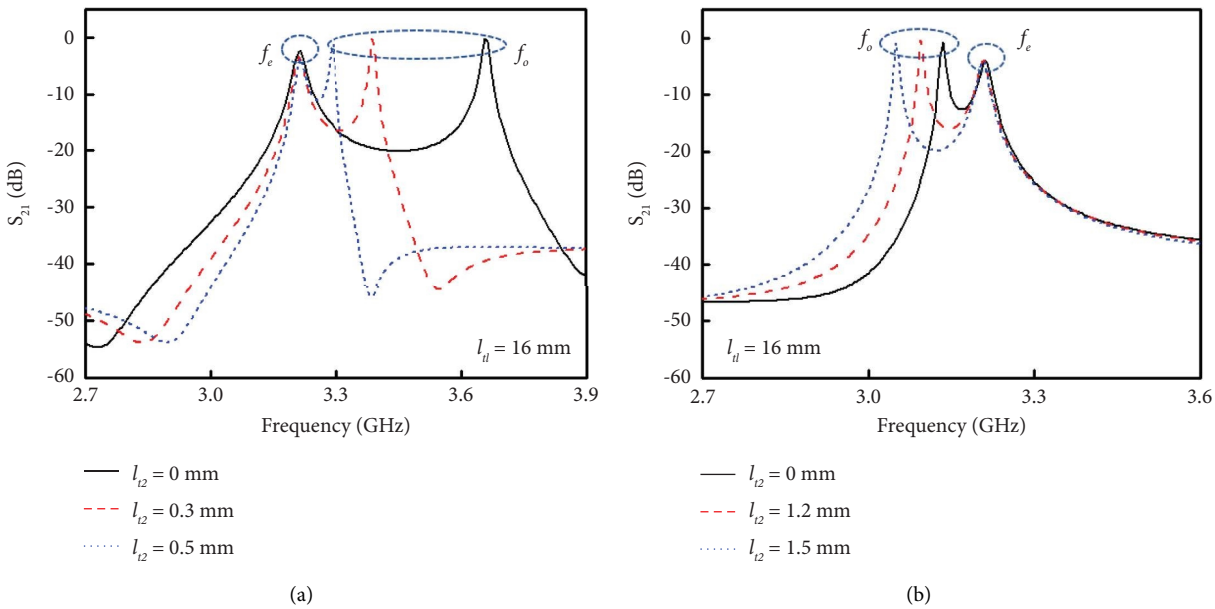

FIGURE 4: Simulated S_{21} in the weak coupling condition for (a) $l_{t2} = 0$ mm, 0.3 mm, 0.5 mm (M dominant coupling), (b) $l_{t2} = 1$ mm, 1.2 mm, 1.5 mm (E dominant coupling).

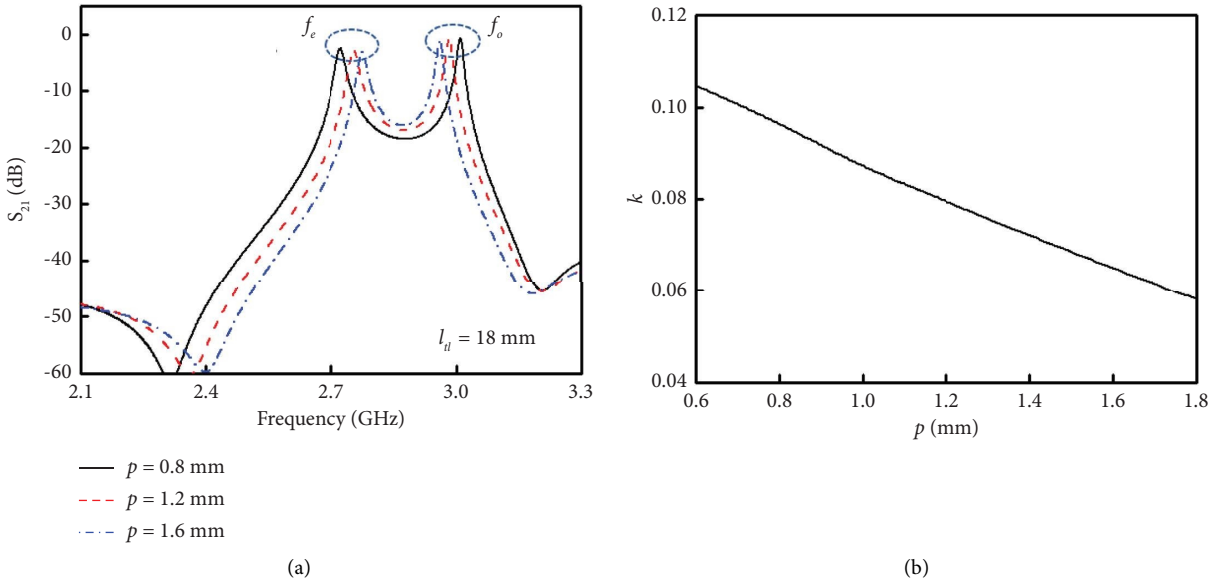

FIGURE 5: Continued.

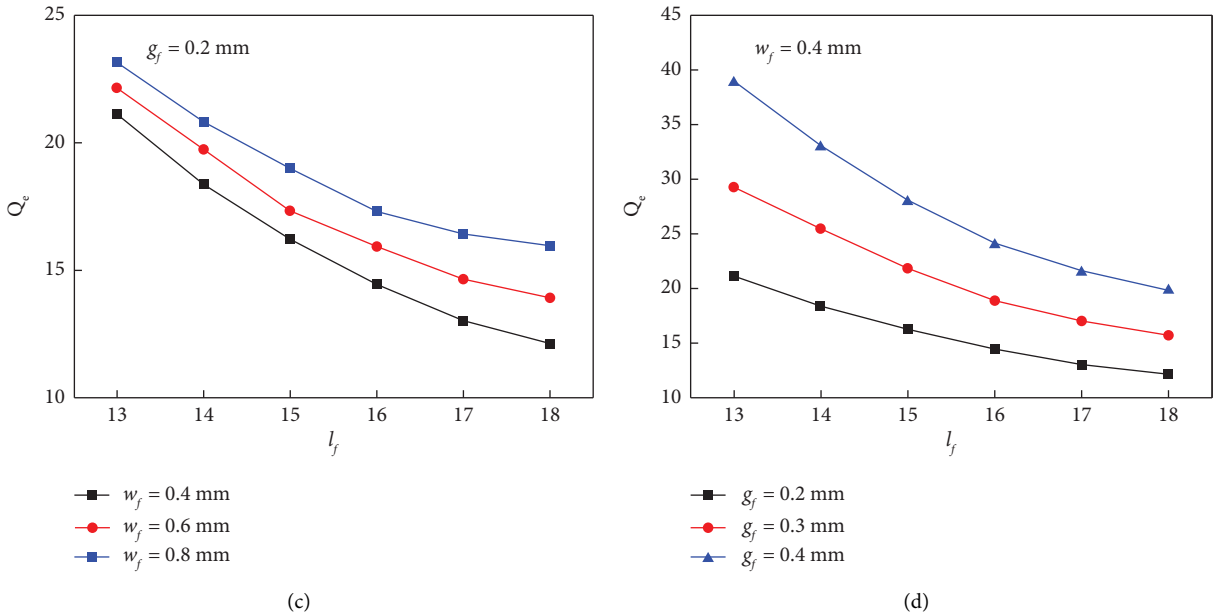

FIGURE 5: (a) Simulated S_{21} in the weak coupling condition for $p = 0.8$ mm, 1.2 mm, and 1.6 mm. (b) The extracted k with respect to p ($l_{t2} = 0$ mm). (c) The extracted Q_e with w_f, l_f ($g_f = 0.2$ mm). (d) The extracted Q_e with g_f, l_f ($w_f = 0.4$ mm).

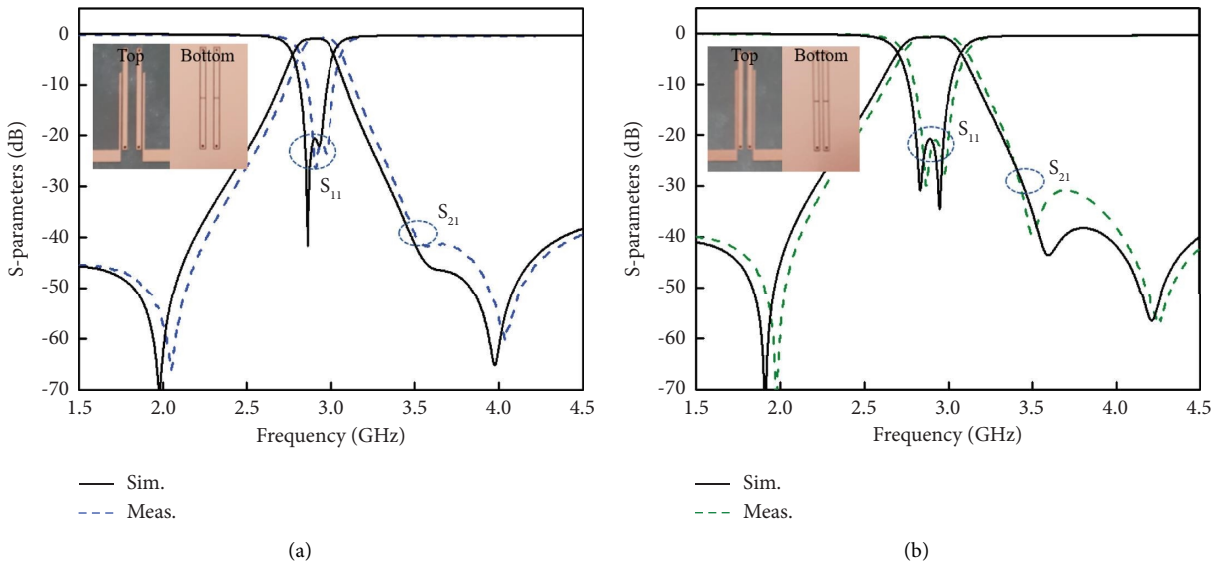

FIGURE 6: Simulated and measured S-parameters for (a) the narrow- and (b) wide-band BPFs.

$$M = \begin{bmatrix} 0 & m_{S1} & 0 & m_{SL} \\ m_{1S} & 0 & m_{12} & 0 \\ 0 & m_{21} & 0 & m_{2L} \\ m_{SL} & 0 & m_{L2} & 0 \end{bmatrix} = \begin{bmatrix} 0 & 1.225 & 0 & 0 \\ 1.225 & 0 & 1.659 & 0 \\ 0 & 1.659 & 0 & 1.225 \\ 0 & 0 & 1.225 & 0 \end{bmatrix}, \quad (5)$$

and the denormalized elements of the general coupling matrix can be obtained by the following equation:

$$k = FBW \bullet m_{12}, Q_e = \frac{1}{FBW \bullet m_{S1}^2}, \quad (6)$$

where FBW is the fractional bandwidth and Q_e is the external quality factor. A highly selective BPF with M-dominant coupling was designed by setting l_{t2} to 0 mm. The simulations shown in Figure 5(a) were executed with weak coupling conditions ($w_f = 0.4$ mm, $g_f = 0.8$ mm, $l_f = 10$ mm) with respect to p. M-coupling in the top layer was more sensitive than E-coupling in the bottom layer with respect to the value of p.

Table 1: Comparison with other works.

	f_r (GHz)	The circuit sizes ($\lambda_g \times \lambda_g$)	Type of resonator	The number of resonators
[10]	2.4	0.37×0.063	Planar	2
[12]	3.4	0.21×0.21	Planar	2
[6]	2.6	0.25×0.053	Vertical	1
This work	2.9	0.29×0.043	Vertical	2

As p was increased, the value of L_m decreased. Therefore, the separation between f_e and f_o decreased accordingly as p was increased, and k can be adjusted as a function of p, as shown in Figure 5(b). Q_e was extracted with respect to w_f, l_f and g_f, as presented in Figures 5(c) and 5(d). From the analysis, the dimensions of the proposed narrow-band BPF (FBW = 3.6%) were calculated ($p = 1.8$ mm, $w_f = 0.4$ mm, $g_f = 0.3$ mm, $l_f = 15.2$ mm). Similarly, the proposed wide-band BPF (FBW = 5.8%) was calculated ($p = 1.0$ mm, $w_f = 0.4$ mm, $g_f = 0.2$ mm, $l_f = 16.3$ mm).

To validate these calculations, the narrow- and wide-band BPFs were fabricated and the measured results were compared to the simulations, as shown in Figure 6. The narrow-band BPF passband RL was measured at less than 20 dB, and the insertion losses (IL) in the simulated and measured filters were 0.99 dB with $f_c = 2.89$ GHz ($FBW = 3.63\%$) and 0.98 dB with $f_c = 2.93$ GHz ($FBW = 3.62\%$), respectively. The simulated and measured wide-band BPF passband RL and IL were 0.72 dB with $f_c = 2.89$ GHz ($FBW = 5.87\%$) and 0.72 dB with $f_c = 2.92$ GHz ($FBW = 5.81\%$), respectively. There was a good agreement between the measured and simulated results.

In addition, TZs were generated on both sides of f_c by both BPFs, as shown in Figures 6(a) and 6(b); the first two TZs were generated by cancelling effects, and the third TZ was generated by the harmonic effects of the distributed transmission line [11]. The locations of TZs are dependent on the amount of coupling between source and VSRR, between two VSRRs, between VSRR and load, and between source and load.

In Table 1, the proposed BPF is compared to other works. The size of the proposed BPF is $0.29\lambda_g \times 0.043\lambda_g$, which is smaller than other planar resonators. It is also clear that the selectivity of the proposed BPF is greater than BPFs using VSRR as the TZs generated from MEMCP.

3. Conclusion

We have introduced two highly selective BPFs, based on VSRRs coupled with MEMCPs. It was shown that E- and M-coupling were dominant in coplanar and microstrip waveguides, respectively, and that M-dominant coupling should be maintained for high selectivity. As a result, narrow- and wide-band BPFs were designed and measured.

Data Availability

The data that support the findings of this study are available from the corresponding author upon reasonable request.

Conflicts of Interest

The authors declare that they have no conflicts of interest.

Acknowledgments

This work was supported in part by the Basic Science Research Program through the National Research Foundation of Korea (NRF), Funded by the Ministry of Education, Republic of Korea (Grant no. NRF-2018R1D1A1B07049347) and in part by Samsung Electronics, Inc.

References

[1] J. D. Baena, R. Marqués, F. Medina, and J. Martel, "Artificial magnetic metamaterial design by using spiral resonators," *Physical Review B*, vol. 69, no. 1, Article ID 014402, 2004.

[2] R. Marqués, F. Mesa, J. Martel, and F. Medina, "Comparative analysis of edge-and broadside-coupled split ring resonators for metamaterial design-theory and experiments," *IEEE Transactions on Antennas and Propagation*, vol. 51, no. 10, pp. 2572–2581, 2003.

[3] F. Aznar, M. Gil, J. Bonache, J. Garcia-Garcia, and F. Martin, "Metamaterial transmission lines based on broad-side coupled spiral resonators," *Electronics Letters*, vol. 43, no. 9, pp. 530–532, 2007.

[4] Z. Troudi, J. Macháč, and L. Osman, "Compact dual-band bandpass filter using amodified hexagonal split ring resonator," *Microwave and Optical Technology Letters*, vol. 62, no. 5, pp. 1893–1899, 2020.

[5] J. Choi, S. Oh, S. Jo, W. S. Yoon, and J. Lee, "Vertical split ring resonator using vias with wide bandwidth and small electrical size," *IEEE Microwave and Wireless Components Letters*, vol. 27, no. 1, pp. 16–18, 2017.

[6] S. Oh, J. Choi, B. Shin, W. S. Yoon, J. Jeong, and J. Lee, "Bandpass filter design based on vertical split-ring resonators," *Electronics Letters*, vol. 53, no. 21, pp. 1412–1414, 2017.

[7] J. Lim, S. Lee, S. Oh et al., "Design of miniaturized vertical split-ring resonator based on coupled coplanar waveguide," *IEEE Microwave and Wireless Components Letters*, vol. 28, no. 9, pp. 753–755, 2018.

[8] Q. X. Chu and H. Wang, "A compact open-loop filter with mixed electric and magnetic coupling," *IEEE Transactions on Microwave Theory and Techniques*, vol. 56, no. 2, pp. 431–439, 2008.

[9] F. Zhu, W. Hong, J. X. Chen, and K. Wu, "Quarter-wavelength stepped-impedance resonator filter with mixed electric and magnetic coupling," *IEEE Microwave and Wireless Components Letters*, vol. 24, no. 2, pp. 90–92, 2014.

[10] J. K. Xiao, M. Zhu, Y. Li, L. Tian, and J. G. Ma, "High selective microstrip bandpass filter and diplexer with mixed electromagnetic coupling," *IEEE Microwave and Wireless Components Letters*, vol. 25, no. 12, pp. 781–783, 2015.

[11] K. Ma, J. G. Ma, K. S. Yeo, and M. A. Do, "A compact size coupling controllable filter with separate electric and magnetic coupling paths," *IEEE Transactions on Microwave Theory and Techniques*, vol. 54, no. 3, pp. 1113–1119, 2006.

[12] J. K. Xiao, M. Zhang, and J. G. Ma, "High selective microstrip bandpass filter and diplexer with common magnetic coupling," *Electronics Letters*, vol. 54, no. 25, pp. 1438–1440, 2018.

[13] V. K. Killamsetty and B. Mukherjee, "Compact triple band bandpass filters design using mixed coupled resonators," *AEU - International Journal of Electronics and Communications*, vol. 107, pp. 49–56, 2019.

[14] J. K. Xiao, X. Ren, and K. M. Guo, "High selective dual-band filtering power divider using self-packaged SISL," *Electronics Letters*, vol. 56, no. 18, pp. 937–940, 2020.

[15] J. S. Hong and M. J. Lancaster, "Couplings of microstrip square open-loop resonators for cross-coupled planar microwave filters," *IEEE Transactions on Microwave Theory and Techniques*, vol. 44, no. 11, pp. 2099–2109, 1996.